Industrial Crops & Products 171 (2021) 113877

Contents lists available at ScienceDirect

Industrial Crops & Products

journal homepage: www.elsevier.com/locate/indcrop

Tuning morphology and structure of non-woody nanocellulose: Ranging between nanofibers and nanocrystals

Ferran Serra-Parareda [a], Quim Tarrés [a,*], José Luis Sanchez-Salvador [b], Cristina Campano [b], M. Àngels Pèlach [a], Pere Mutjé [a], Carlos Negro [b], Marc Delgado-Aguilar [a]

[a] LEPAMAP-PRODIS Research Group, University of Girona, C/ Maria Aurèlia Capmany, 61, 17003, Girona, Spain
[b] Department of Chemical Engineering and Materials, University Complutense of Madrid, Avda. Complutense s/n, 28040, Madrid, Spain

ARTICLE INFO

Keywords:
Nanostructured cellulose
Cellulose nanofibers
Cellulose nanocrystals
Annual plants
Hemp
Sisal
Jute
TEMPO-mediated oxidation

ABSTRACT

Due to the increasing interest on lignocellulosic nanomaterials, alternative raw materials to wood sources have been explored. In this sense, annual plants can represent an important source of lignocellulose which may be used for cellulose nanofibers (CNFs) production. The present work aims at highlighting the virtues of three different non-woody resources (jute, sisal and hemp) as raw material for the production of TEMPO-mediated oxidized CNFs. The fibrillation stage was carried out by means of high-pressure homogenization (HPH), sequencing the process to obtain the initial, intermediate and final characteristics. Interestingly, it was found that while wood-based TEMPO-mediated oxidized CNFs lead highly fibrillated structures and thick gels, the obtained CNFs in this work exhibited a structure similar to cellulose nanocrystals (CNCs), particularly at high oxidation degrees, as rod-like morphologies were observed. Nonetheless, differences were observed between the selected raw materials, which was attributed to the differences on their relative recalcitrance. In addition, the rheological evaluation indicated that hemp CNFs tended to a Newtonian behavior, as flow behavior index tended to 1, leading to suspensions radically different to those obtained from wood sources. Further, the rheological behavior of the obtained nanocellulose suspensions has been found to correlate with the 2D fractal dimension of the nanostructured cellulose. Overall, the present work shows the feasibility of using non-woody plants as raw material for nanostructured cellulose production, with interesting characteristics unconceivable with wood resources.

1. Introduction

Lignocellulose, the most abundant bio-based material, is constituted by cellulose, hemicellulose, and lignin, which acts as a binder of cellulose and hemicellulose and provides dimensional stability to lignocellulosic fibers (Ebringerová and Heinze, 2000; Morales et al., 2014; Boufi et al., 2016; Song et al., 2016). Traditionally, lignocellulose has been extracted from wood and plants for several applications, including papermaking, fiberboards, natural fiber reinforced composites, biofuels, and additives for many other value-added sectors (Torres et al., 2012; De France et al., 2017; Blanco et al., 2018; Domínguez-Robles et al., 2018; Oliver-Ortega et al., 2019; Trakulvichean et al., 2019). This extraction process is usually performed by means of single-step or multi-step treatments, having as main objective the softening and removal of part of the lignin and other unwanted compounds, which promote the release of individualized fibers. Some examples of processes for lignocellulose extraction can be found in the literature, and usually consist of mechanical, thermal, chemical, or enzymatic treatments (Sjöström and Westermark, 1999; Sundholm, 1999; Ek et al., 2017; Lin et al., 2018; Pirich et al., 2020).

Due to the increasing interest on lignocellulosic materials, and the desire of maintaining this sector as sustainable as possible, alternative raw materials have been widely explored, particularly those coming from non-woody plants as jute, sisal, cotton, flax or hemp (Sridach, 2010; Hubbe, 2014; Gontard et al., 2018; Abd El-Sayed et al., 2020). As in the case of wood, non-wood plants contain the same components, but their content and physicochemical characteristics (i.e. fibril length, fibril width, microfiber angle, lumen diameter, cell wall thickness, crystallinity) are different (Ludueña et al., 2013). Compared to wood, non-wood plants have generally lower lignin contents (Marques et al., 2010; Tarrés et al., 2017c), shorter growing cycles with moderate irrigation requirements, annual crops and a high annual yield of cellulose.

* Corresponding author.
E-mail address: joaquimagusti.tarres@udg.edu (Q. Tarrés).

https://doi.org/10.1016/j.indcrop.2021.113877
Received 4 May 2021; Received in revised form 23 July 2021; Accepted 26 July 2021
Available online 29 July 2021

These characteristics made these raw materials very interesting to be used as raw material to produce nanosized fibers.

Out of these fibers, jute fiber is one of the major under-utilized agricultural raw materials with a cellulose content around 70 %. It grows in hot and humid climates of the equatorial, tropical and the sub-tropical zones and is a fast-growing annual plant (it reaches about 2.5–3 m in height within 4–6 months) whose fibers are extracted from the ribbon of the stem (Ramamoorthy et al., 2015; Saleem et al., 2020). They are easily available in fabric and fiber forms with good mechanical and thermal properties. Jute has wood-like characteristics, as it is a bast fiber with a high aspect ratio, high strength to weight ratio and good insulation properties (Gon et al., 2013). Due to its heterogeneity and crystallinity, however, direct utilization of the biomass is extremely low.

Other non-wood plant easily cultivated, mainly in Brazil and East Africa, with a significant amount of cellulose is sisal, one of the most widely used natural fibers (Sharma and Chaudhary, 2020). Sisal has short renewal times and grows wild in the hedges of fields and railway tracks. These fibers have many advantages, such as high tenacity and tensile strength, as well as resistance to abrasion, acid, alkali, sea water, corrosion, and so on (Rohit and Dixit, 2016).

Another notable bast fiber crop is hemp, one of the fastest growing plants cultivated in a temperate climate (Ramamoorthy et al., 2015). Hemp is known to provide an excellent mechanical strength and young's modulus, with a cellulose content around 55–72 % and low lignin content under 5 % (Alila et al., 2013; Rohit and Dixit, 2016).

The variation in non-wood plants is clearly illustrated in terms of length, microfibril angle, amount of non-cellulosic residues and quality. Therefore, the isolation of nanosized fibers from different lignocellulosic biomass sources is relevant in order to efficiently compare and exploit these resources (Siqueira et al., 2010; Deepa et al., 2011; Alila et al., 2013).

These nanosized cellulose-based materials are generally known as nanocellulose (NC), and two main top-down structures have been reported to the date: cellulose nanofibers (CNFs) and cellulose nanocrystals (CNCs) (Habibi et al., 2010; Dufresne, 2018). CNFs are nanosized fibers containing both amorphous and crystalline regions, leading to strong but flexible structures, which provide high dimensional stability in the form of stable entangled 3D-structured networks. Depending on the treatment intensity, CNF suspensions may also contain microsized fibers, being microfibrillated cellulose (MFC) a common term to refer to suspensions containing both micro and nanosized fibers. On the other hand, CNCs are extracted from fibers after an almost complete dissolution of the amorphous cellulose fractions, by means of either enzymatic or acid hydrolysis. The resulting rod-like structures also exhibit nanosized diameters and high surface area, but their ability to form stable 3D-structured networks is limited and some crosslinking agents may be used for nanocellulose-based aerogels and hydrogels (Bondeson et al., 2006; Isogai et al., 2011; Nascimento et al., 2016; De France et al., 2017; Campano et al., 2021). This lower stability of the 3D structures may be attributed to the low entanglement capacity of CNCs, although percolation has been already proved for such nanosized cellulose-based materials when embedded in polymer matrices (Favier et al., 1997). Although plants are the major contributor of cellulose, NC can be also obtained by means of bottom-up approaches, as is the case of bacterial cellulose (BC). This kind of NC is completely different to CNFs and CNCs, as it is grown from bacteria (Iguchi et al., 2000).

CNF production encompasses fibrillation processes for fiber individualization, including microfluidization, high-pressure homogenization or grinding (Abdul Khalil et al., 2014). However, these techniques are usually energy consuming and fibers need to be previously treated, which facilitates the individualization process, as they enhance fiber swelling, and provide functional groups at the CNFs surface (Isogai et al., 2011; Spence et al., 2011; Rodionova et al., 2013; Kekäläinen et al., 2014). Among the different pretreatments, there are few that have gained relevance among the scientific community, such as enzymatic hydrolysis (Henriksson et al., 2007; Pääkko et al., 2007; Tarrés et al., 2016b), TEMPO-mediated oxidation (Saito et al., 2007; Fujisawa et al., 2011), or carboxymethylation (Duker et al., 2008; Ankerfors et al., 2013). One of the most widely used chemical pretreatments in the production of CNFs is TEMPO-mediated oxidation. This pretreatment is based on the regioselective oxidation of C6 primary hydroxyl of the cellulose chain (Sun et al., 2005; Sbiai et al., 2011). The introduction of this negatively charged group into the fibrils generates electrostatic repulsion forces that promote bundles' separation. In this sense, an increase in the degree of oxidation, which means a higher carboxyl content, allows reaching a higher degree of nanofibrillation at a certain applied energy during fibrillation.

The influence of the carboxyl group content and the mechanical treatments on the properties of the resulting nanofibers has been a topic of great interest, although wood fibers have been typically used (Besbes et al., 2011; Serra et al., 2017). However, there are few studies dealing with the production of TEMPO-oxidized CNFs from annual plants (Cao et al., 2013; Puangsin et al., 2013; Pennells et al., 2020). As stated above, annual plants usually exhibit low lignin contents compared to wood (Marques et al., 2014; Chokshi et al., 2020). The removal of lignin is strongly recommended prior to TEMPO-mediated oxidation in order to prevent undesired side-reactions, making low-lignin content sources interesting for such kind of processes (Wen et al., 2019; Jiang et al., 2020). Indeed, delignification processes can be conducted at lower intensities, preventing structural and irreversible damages to the fibers and, in addition, the structural differences between annual plants and wood, particularly in terms of crystallinity, may confer the resulting CNFs of interesting characteristics, such as lower viscosity or higher crystallinity.

In the present study, commercial bleached jute, sisal, and hemp pulps were subjected to TEMPO-mediated oxidation at different oxidation degrees. The effects of oxidation were evaluated in terms of carboxylic groups formed, as well as morphological changes. Besides, the oxidized fibers were subjected to increasing high-pressure homogenization sequences (pressure and cycles), aiming at determining intermediate and final CNF characteristics. The present work provides important information to determine the influence of the chemical composition and morphology of the fibers on the changes that they are subjected at TEMPO-mediated oxidation and the subsequent nanofibrillation process, as well as the resulting characteristics of the obtained nanostructures, which may be categorized as CNFs or CNCs. For the first time, the correlation between 2D fractal dimension, morphological characteristics, treatment conditions, rheological behavior and CNF/CNCs characteristics (i.e. surface area, cationic demand) are tackled jointly and comprehensively analyzed. Further, the differences on the resulting nanocellulose characteristics are linked to the chemical and structural characteristics of the starting fibers, which have been reported to influence the relative recalcitrance of biomass. The present work brings to the light great opportunities of annual plants as raw material for CNF and CNC production by means of a common process (TEMPO-mediated oxidation), adding versatility to a plausible industrial scale production with no need of two separate production lines for CNFs and CNCs, as morphology and structural characteristics could be tailored by means of adjusting oxidation and fibrillation conditions.

2. Experimental section

2.1. Materials

Bleached jute, sisal, and hemp pulps were kindly provided by Celesa (Spain) and used as raw material of CNFs. The chemical reagents involved in TEMPO-mediated oxidation, as well as those used for the characterization of fibers and nanofibers, were obtained from Merck (Spain). All reagents were used without further purification.

2.2. TEMPO-mediated oxidation

TEMPO-mediated oxidation was carried out at pH 10 according to the widely reported and previously used method (Saito et al., 2007). Two levels of oxidation were selected as function of the oxidizer amount (OA): 5 and 15 mmol/g. Further details of the method can be found in the literature (Fujisawa et al., 2011; Serra et al., 2017). The reaction was stopped by means of intense washing of the fibers, followed by filtration until neutral pH was achieved. The oxidized fibers were kept at 4 °C in hermetic plastic bags for further processing and characterization.

2.3. High-pressure homogenization of oxidized fibers

The fibrillation process of the TEMPO-mediated oxidized fibers was conducted at 1 wt% consistency by means of high-pressure homogenization (HPH) in a laboratory scale high-pressure homogenizer NS1001 l PANDA 2K-GEA (GEA Niro Soavy, Italy). With the purpose of monitoring the fibrillation process, an incremental sequence was designed, taking samples at five different stages of the HPH process (Table 1).

2.4. Characterization of the neat and TEMPO-oxidized jute, sisal and hemp fibers

Untreated and TEMPO-mediated oxidized fibers were characterized in terms of morphology and carboxyl content. Further, the chemical composition and the crystallinity index of untreated fibers were determined.

Klason and soluble lignin, cellulose and hemicellulose contents were measured in the raw materials. Although the extractives content is not reported in the manuscript, the extractive-free samples are required for determining the rest of the constituents. Extractives were removed from the samples by Soxhlet extraction according to TAPPI T204. Total lignin, hemicellulose and cellulose of raw materials were obtained following NREL/TP-510-42618. Tests were performed in triplicate.

Crystallinity index (CrI) was obtained by X-ray diffraction (XRD) spectra. A Philips X'Pert MPD X-Ray diffractometer was used with an auto-divergent slit fitted with a graphite monocromator, Cu-Kα radiation and operated at 45 kV and 40 mA. XRD patterns were recorded in a range from 3 to 80° at a scanning speed of 1.5 °/min. Segal's method was used to determine CrI (Segal et al., 1959). Three scans per sample were performed.

Carboxyl content of the fibers, both untreated and TEMPO-mediated oxidized, was calculated by conductimetric titration, as reported elsewhere (Serra et al., 2017). This parameter was used as indicative of the oxidation degree. Carboxyl content was determined in triplicate.

The morphology of the jute, sisal and hemp fibers, both untreated and TEMPO-mediated oxidized, was assessed in a MorFi Compact Analyzer (TechPap, France) equipped with a CCD video camera and the software MorFi v9.2. The morphology was determined over four diluted fiber samples per material. Further, samples were observed by optical microscopy (OM) using a Zeiss Axio Lab.A1 optical microscope under x5 magnification.

2.5. Characterization of CNFs

Cationic demand (CD) was determined by means of back titration in a particle charge detector (Mütek PCD 04, BTG), as it has been extensively reported in previous works (Tarrés et al., 2016a; Serra-Parareda et al., 2021). PolyDADMAC with a molecular weight (Mw) of 107 kDa was selected in order to avoid polymer penetration into the CNF structure (Zhang et al., 2016).

The nanofibrillation yield was determined by centrifuging a diluted CNF suspension (0.2 wt%). The nanofibrillated fraction, contained in the supernatant, was isolated from the non-nanofibrillated, which was assumed to get retained in the sediment. The recovered sediment was oven-dried until constant weight and referred to the initial dry mass, obtaining the non-nanofibrillated fraction. The nanofibrillated fraction was calculated by difference.

Transmittance of CNF suspensions was measured by means of spectrophotometry using distilled water as background. The consistency of the CNF gels was set at 0.1 wt% and the wavelength, between 400 and 800 nm. The equipment was a UV–vis Shimadzu spectrophotometer UV-160A.

The morphology of the obtained nanofibers was analyzed by transmission electron microscopy (TEM) performed at the Centro Nacional de Microscopía Electrónica (Madrid, Spain) with a JEM 1400 microscope from JEOL (Tokyo, Japan) and sample was prepared according to a previously reported procedure (Campano et al., 2020). Projected fractal dimension (D_2) was measured on the TEM images. The acquired images were processed and analyzed through the Fiji distribution of ImageJ 1.53k15. Images were firstly edited to achieve a good definition and high contrast of CNF borders. They were first converted into 8-bit images and then submitted to a bandpass filter and background subtraction to minimize the effect of impurities and irregularities in the images. They were, then, binarized through an auto threshold and corrected with a Close filter (Campano et al., 2021). Elements in the images were selected individually and copied into a separate file. The fractal analysis was performed with the Fractal Box Count plugin. To reduce processing times, this procedure was automatized through a script.

The gel point methodology based on the sedimentation of the fibers was used to determine the aspect ratio of the nanofibers (Varanasi et al., 2013). On this occasion, a new simplified method was used based on replacing the derivative at the origin of the curve initial concentration ($Ø_o$) versus the ratio between the height of the sediment (H_s) and the initial height of the suspension (H_o), by an increment between an initial concentration $Ø_o(i)$ and a theoretical concentration of zero, $Ø_o(0)$. Therefore, the derivative initially proposed by the gel point method can be approximated to the quotient between the difference in concentrations and the variation in the height ratio. Where, both $Ø_o$ (0) and (H_s/H_o (0)) are considered to be zero.

$$Gel\ Point = \left(\frac{dØ_0}{d\left(\frac{H_s}{H_0}\right)}\right) \approx \frac{Ø_0(i) - Ø_0(0)}{\left(\frac{H_s}{H_0}(i)\right) - \left(\frac{H_s}{H_0}(0)\right)} = \frac{Ø_0(i)}{\frac{H_s}{H_0}(i)} \quad (1)$$

Sample preparation for gel point determination was performed with a CNF suspension between 0.1 and 0.3 %w/w with deionized water that was shaken for 10 min. The selection of the initial concentration was made to obtain a sediment height around 4–12 % of the total height. 200 µl of 0.1 wt% crystal violet was added during shaking to favor visualization of the sediment (Sanchez-Salvador et al., 2020). Then, 250 mL of the suspension was allowed to stand in a graduated cylinder until the sediment reached a stable value indicating complete deposition of the fibers. The values obtained from the gel point study were related to the aspect ratio (Varanasi et al., 2013). For this purpose, a fiber density of 1500 kg/m3 was assumed and the crowding number theory was used (Martinez et al., 2001):

$$Aspect\ ratio = 6.0 * \left(\frac{Gel\ Point}{1000}\right)^{-0.5} \quad (2)$$

The shear-thinning behavior of the CNF suspensions was determined

Table 1
Designed HPH sequence.

HPH sequence	300 bar (cycles)	600 bar (cycles)	900 bar (cycles)
3-0-0	3	0	0
3-1-0	3	1	0
3-3-0	3	3	0
3-3-1	3	3	1
3-3-3	3	3	3

by means of a PCE-RVI 2 V1L rotational viscosimeter (PCE Instruments, Germany) equipped with the L3 spindle and rotating from 0.3–200 rpm. The shear rate was varied from 0.21–141.24 s^{-1} and apparent viscosity was recorded (η). Conditions related to spindle shape, dimensions, vessel and rotational speed were considered, obtaining a ratio between the diameter of the vessel and the spindle of 1.2 (Filipova et al., 2020). Apparent viscosity values were plotted as function of the shear rate and fitted to the Ostwald de Waele relationship (Eq. 3) (Lasseuguette et al., 2008).

$$\eta = K \cdot \gamma^{n-1} \quad (3)$$

where K is the viscosity coefficient (consistency factor) and n is the flow behavior index, which are calculated from the exponential regression (Loranger et al., 2012).

All tests were carried out with five samples of each material. The reported results in the next section are the average of these five test runs.

3. Results and discussion

3.1. Effects of TEMPO-mediated oxidation

Due to the reaction mechanism of TEMPO-mediated oxidation, the carboxyl groups concentration on oxidized fibers serves as useful indicator of their oxidation degree. Table 2 shows the obtained carboxyl content (CC) as function of the oxidizer amount (OA), namely NaClO per gram of fiber, for the three tested pulps.

Neat jute, sisal, and hemp fibers exhibited a similar CC, ranging between 42 and 54 μeq/g. These values are similar to those of other bleached wood fibers such as eucalyptus or spruce, with values below 60 μeq/g (Besbes et al., 2011; Oliaei et al., 2020). According to the reaction mechanism of TEMPO-mediated oxidation, one mol of the primary hydroxymethyl group in carbon 6 of the cellulose chain is converted to one mol of C6 carboxylate group, through an intermediate reaction leading to the formation of C6 aldehyde with a consumption of 2 mol of NaClO (Saito et al., 2007). As expected, at increasing OA, the CC was enhanced, reaching values near to 800 and 1400 μeq/g for NaClO additions of 5 and 15 mmol/g, respectively, and regardless the fiber origin. The obtained CC was of the same order of magnitude than in the case of bleached wood fibers, where values around 800 and 1500 μeq/g for 5 and 15 mmol/g of NaClO, respectively, have been reported (Tarrés et al., 2017a). This equivalence between bleached wood fibers and the ones from the present study comes from the similarities on chemical compositions. Although cellulose and hemicellulose contents may differ from each other, none of them contained lignin or its presence was residual. Indeed, lignin has been reported to limit the conversion of hydroxyl groups from CH_2OH to carboxyl during TEMPO-mediated oxidation, which clearly affects the reaction yield and performance (Jiang et al., 2020).

TEMPO-mediated oxidation has been also reported to have a direct impact on fiber morphology (Osong et al., 2016). Indeed, this oxidative treatment is intended to incorporate more voluminous groups (COO-) that may impart repulsive forces to deconstruct the hierarchical structure of cellulose, while increasing fiber swelling and promoting the release of micro/nanofibrils, as well as decrease fiber length to promote their pass through the pressure chambers of high-pressure homogenizers (Saito and Isogai, 2004; Isogai et al., 2011; Levanič et al., 2020). Table 3 shows the morphological characteristics of the neat and TEMPO-mediated oxidized jute, sisal and hemp fibers, prior to the HPH process.

Regardless the fiber source, arithmetic length was strongly shortened at oxidation rates of 5 mmol/g NaClO, resulting in a reduction of about 60 %, which was further decreased at 15 mmol/g of OA. Extension of NaClO consumption to 15 mmol/g only resulted in approximately 10 % more reduction in arithmetic length with regard to the initial fiber length. As expected, this effect was also observed in the length weighted in length. However, the impact of OA on the fines content was more pronounced, as it increased by 50 and 75 % for 5 and 15 mmol/g of OA, respectively. As detailed in the previous section, the calculation of the arithmetical length and the length weighted in length do not consider the fines morphology, as they are directly classified as fibers shorter than 75 μm. This notable increase on the fines content clearly indicate that fibers oxidized at 15 mmol/g are much shorter than those oxidized at 5 mmol/g, and that the obtained values of l_a and l^l_w must be contextualized with the rest of the morphological parameters. This fiber shortening clearly indicate a remarkable depolymerization of the cellulose chains, in turn caused by the removal of part of the hemicellulose, amorphous cellulose, and residual lignin (Okita et al., 2009; Shinoda et al., 2012). The reduction on fiber diameter is attributed to enhancement of their surface charge due to the introduction of voluminous and negatively charged COO^- groups, which generates strong repulsive forces that may increase fiber swelling and, thus, the release of micro/nanofibrils (Isogai et al., 2011; Levanič et al., 2020). This reduction occurs progressively in the case of sisal, while in the case of Hemp fibers at 5 mmol/g of OA it is more pronounced. On the contrary, in the case of Jute fibers, the most pronounced reduction in diameter is experienced when OA is increased from 5 to 15 mmol/g. Indeed, TEMPO-mediated oxidation has been already reported to have different effect on fiber morphology depending on the recalcitrance of the fiber source. Recalcitrance, an emerging property of the molecular and structural complexity of the plant cell walls, can be generally described as those features of biomass that increase energy requirements for bundles fibrillation (McCann and Carpita, 2015). Pinto et al. (2019) already observed that recalcitrance had a notable effect on the resulting morphology of TEMPO-oxidized fibers, as notable significant differences were observed between eucalyptus and sugarcane bagasse.

The morphological changes were further assessed by means of

Table 2
Evolution of carboxyl content with the oxidizer amount for jute, sisal and hemp fibers.

	CC (μeq/g)		
OA (mmol/g)	Jute	Sisal	Hemp
0	47 ± 2	42 ± 3	54 ± 3
5	785 ± 12	790 ± 19	803 ± 21
15	1483 ± 67	1371 ± 43	1363 ± 58

Table 3
Morphological characteristics of neat and TEMPO-mediated oxidized jute, sisal and hemp fibers.

Fiber source	OA (mmol/g)	l_a (μm)	l^l_w (μm)	d (μm)	Coarseness (mg/m)	F (%)	l^l_w/d
Jute	0	566 ± 3	870 ± 7	24.6 ± 0.7	0.249 ± 0.005	26 ± 1	35.4
Sisal		449 ± 37	955 ± 31	21.6 ± 0.6	0.353 ± 0.062	22 ± 2	44.2
Hemp		551 ± 5	1007 ± 25	25.4 ± 0.4	0.370 ± 0.006	28 ± 2	39.6
Jute	5	213 ± 5	295 ± 7	23.8 ± 0.3	0.056 ± 0.013	50 ± 5	12.4
Sisal		185 ± 1	270 ± 1	19.9 ± 0.2	0.098 ± 0.006	46 ± 1	13.6
Hemp		226 ± 5	396 ± 15	21.5 ± 0.8	0.147 ± 0.033	46 ± 1	18.4
Jute	15	174 ± 5	241 ± 9	17.1 ± 0.2	0.050 ± 0.010	78 ± 6	14.1
Sisal		178 ± 6	266 ± 32	18.9 ± 0.6	0.036 ± 0.006	76 ± 6	14.1
Hemp		192 ± 2	304 ± 4	19.1 ± 0.4	0.075 ± 0.013	72 ± 3	15.9

la: arithmetical length; lwl: length weighted in length; d: diameter; f: fines content.

optical microscopy (Fig. 1), where a significant reduction on fiber length and diameter can be observed, as well as the increase on surface fibrillation. This surface fibrillation is supported by the coarseness values from Table 3. The oxidation of sisal fibers, which exhibited an initial coarseness of 0.353 mg/m, was reduced to 0.098 and 0.036 mg/m for 5 and 15 mmol/g of OA, respectively. This pattern was repeated in the case of jute and hemp fibers, where reductions of about the 80 % of the linear mass were observed for a 15 mmol/g NaClO addition. These results could indicate that at least a fraction of the cellulose fibers have been individualized into nanofibrils after extensive TEMPO-mediated oxidation pretreatment. The partial self-release or self-fibrillation of the nanofibrils during TEMPO-mediated oxidation is possible, when the surface charge is sufficient, which occurs at high oxidation rates (Sjöstedt et al., 2015; Gorur et al., 2020). As stated above, recalcitrance of the material may be determinant on the resulting morphology of the oxidized fibers at a certain oxidation level. Indeed, at moderate oxidation degrees (5 mmol/g of OA), hemp exhibited shorter and significantly more individualized fibers (Fig. 1f), rather than in the case of jute or sisal (Figs. 1d and 1e, respectively). The effect of the oxidative process becomes apparent in the optical microscopy images, particularly in Fig. 1g, h, and i, corresponding to sisal, hemp and jute oxidized with 15 mmol/g of NaClO, respectively. Concretely, in the case of sisal and hemp (Fig. 1h and i, respectively) some fine and well-defined particles can be observed, indicating the premature release of micro/nanosized slender structures.

3.2. Characterization of cellulose nanofibers

As detailed above, the characterization of the obtained CNFs consisted of morphological, rheological and surface charge measurements, as function of the fiber source, the oxidation intensity and the HPH sequence.

The obtained CNFs exhibited a high nanofibrillation yield and transmittance at 600 nm (Table 4). The three fiber sources (jute, sisal, and hemp) achieved nanofibrillation yields close to 100 % (labelled as > 95 %) with just 3 cycles at 300 bar when they were oxidized with the maximum amount of oxidizer (15 mmol/g), while lower values were achieved for lower OA (5 mmol/g).

Table 4
Nanofibrillation yield and transmittance at 600 nm of the obtained CNF at different HPH intensities.

OA (mmol/g)	HPH sequence	Nanofibrillation yield (%)			Transmittance at 600 nm (%)		
		Jute	Sisal	Hemp	Jute	Sisal	Hemp
5	3-0-0	69.40	59.87	28.01	68.4	55.6	25.9
	3-1-0	90.53	68.33	34.43	87.7	65.1	29.9
	3-3-0	> 95	86.11	45.39	95.9	83.1	37.7
	3-3-1	> 95	> 95	53.50	96.1	91.4	44.0
	3-3-3	> 95	> 95	58.15	97.5	95.6	54.4
15	3-0-0	87.81	90.12	87.12	90.8	69.3	66.3
	3-1-0	> 95	> 95	93.46	95.5	79.1	75.9
	3-3-0	> 95	> 95	> 95	97.7	89.7	88.2
	3-3-1	> 95	> 95	> 95	99.7	93.9	92.9
	3-3-3	> 95	> 95	> 95	99.7	95.8	95.1

> 95 %: no sedimentation.

Those values of nanofibrillation yield labelled as > 95 % indicate that accounted for values higher than 95 %, as no sedimentation was observed after centrifugation.

Light transmittance is strongly related to nanofiber size and their ability to scatter light (Fujisawa et al., 2011; Isogai et al., 2011). From the visible spectrum (380–750 nm), the light transmittance of 0.1 wt% CNF suspensions at 600 nm was selected and used for comparison purposes. As expected, at lower nanofibrillation yields, lower transmittances were obtained, as non-nanofibrillated or thicker fibers cause a higher scattering of the incident light, thus reducing the transmittance value (Parit et al., 2018). Both nanofibrillation yield and light transmittance consist of indirect measurements that might be correlated with CNFs morphology. Indeed, it is expected that highly fibrillated CNFs may present a narrow length and width distribution, particularly if they exhibit high light transmittance.

The influence of HPH sequence and the oxidation degree was

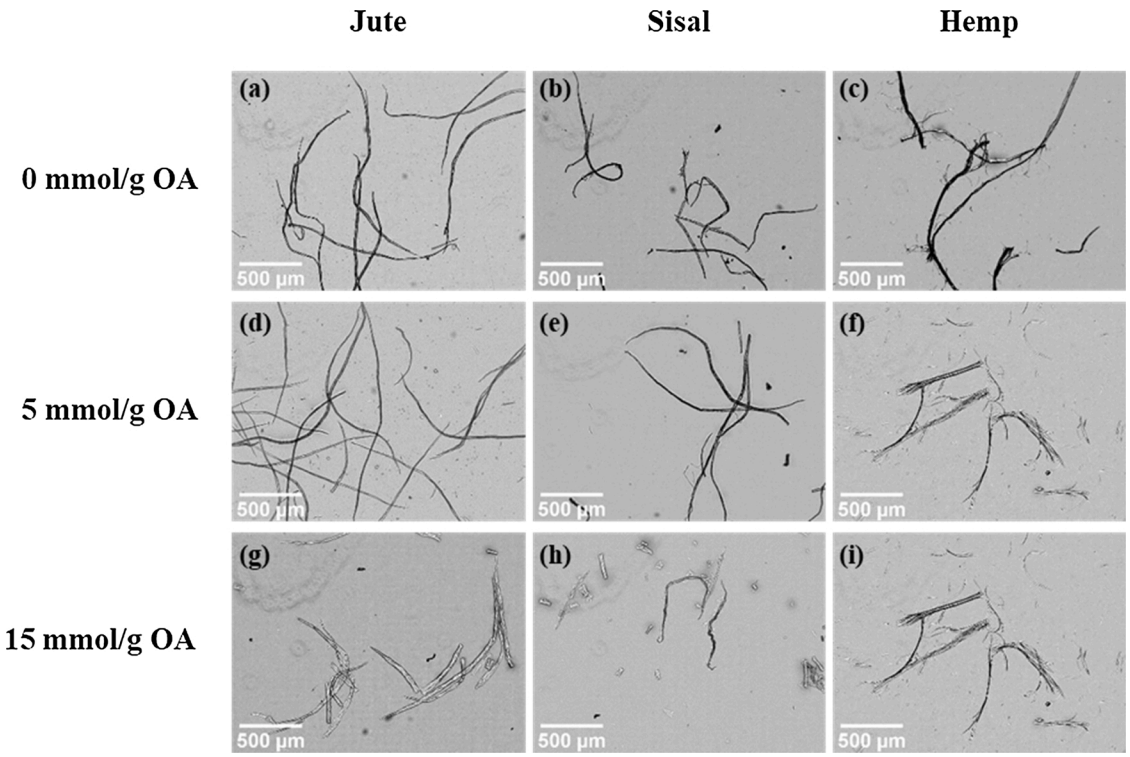

Fig. 1. Optical micrographs of neat and TEMPO-mediated oxidized sisal, hemp and jute fibers.

assessed by means of TEM images (Fig. 2), where CNFs of jute, sisal and hemp, both at 5 and 15 mmol/g of OA and subjected to HPH sequences of 3-0-0, 3-3-0 and 3-3-3 can be observed. The rest of the TEM images (sequences 3-1-0 and 3-3-1) are provided as supplementary material (Fig. S1).

For all cases, the effect of the oxidation degree became apparent, as at low homogenization intensity (i.e. HPH sequence 3-0-0), fiber bundles were clearly observed for those fibers oxidized at 5 mmol/g of NaClO, while individualized and nanosized fibers were already found at the highest oxidation degree. Indeed, such bundles were still present at the severest conditions of HPH (3-3-3) for an OA of 5 mmol/g, bringing to the light the relevance and impact of the TEMPO-mediated oxidation on the final characteristics of CNFs (Saito and Isogai, 2004; Patiño-Masó et al., 2019). Focusing on the morphological characteristics of the obtained CNFs, it can be clearly seen that jute led to longer CNFs, generating entangled networks although being suspended in water. This was not observed in the case of hemp and sisal, particularly at the highest oxidation degree, where shorter and apparently more rigid CNFs were found. Indeed, the obtained structures could indicate that they are CNCs rather than CNFs (Isogai and Zhou, 2019; Campano et al., 2020). As previously discussed, TEMPO-mediated oxidation has a direct impact on fiber morphology, particularly in terms of length and diameter. However, the extent of this effect appeared to be different depending on the fiber source. This could be attributed to the initial characteristics of the

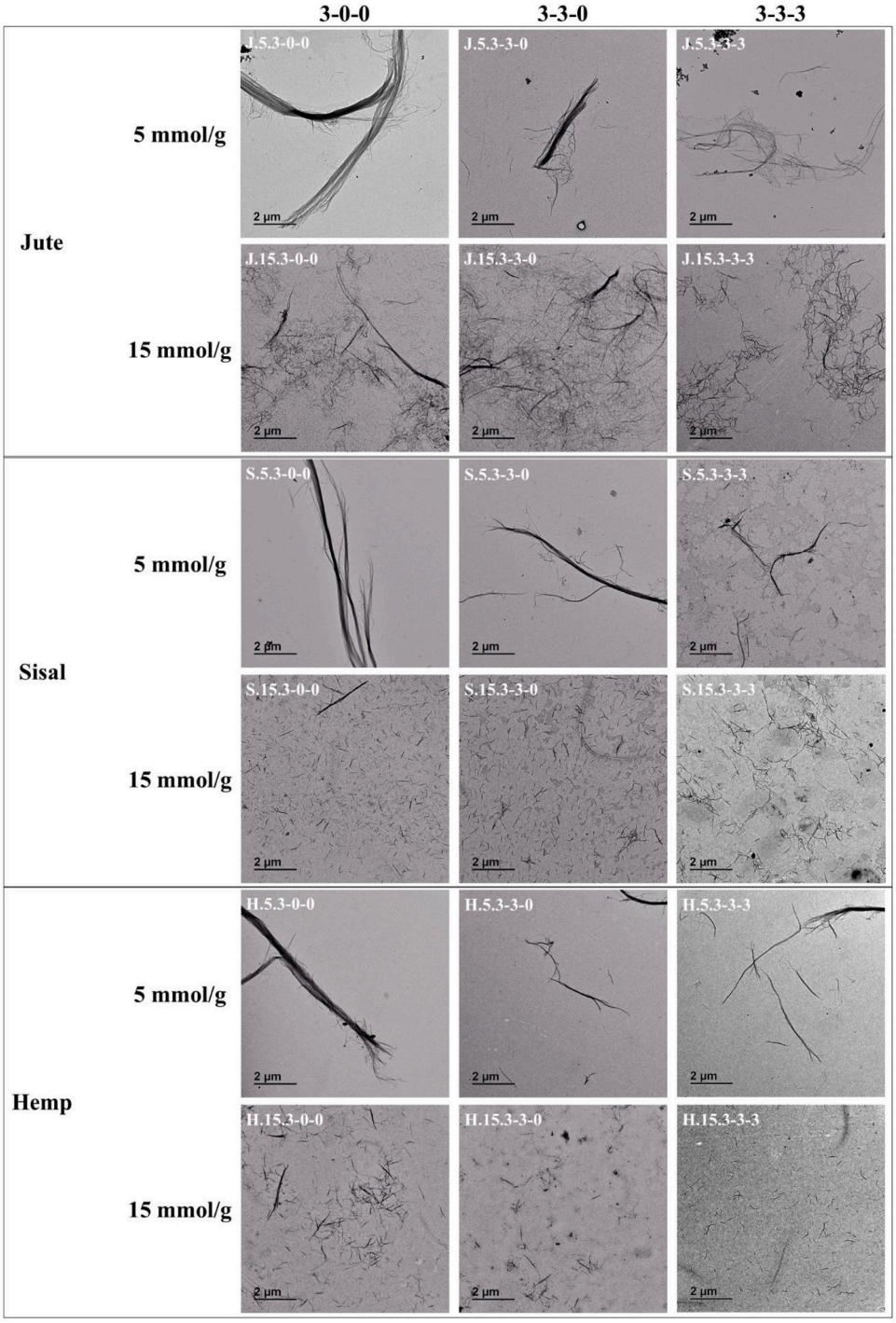

Fig. 2. TEM images of the obtained CNFs as function of the oxidation degree and the HPH sequence.

fibers, particularly the crystallinity degree, chemical composition and, thus, their recalcitrance (McCann and Carpita, 2015; Pinto et al., 2019). The crystallinity of neat jute, sisal, and hemp fibers accounted for 77.8, 75.9 and 75.8 %, respectively. These crystallinities are of the same magnitude and, apparently, it might not explain the differences on the resulting morphology of the obtained CNFs. However, jute fibers exhibited a slightly higher amount of lignin than sisal and hemp, accounting for 6.9, 5.0 and 3.4 wt%, respectively. In addition, the hemicellulose content of hemp fibers (5.8 wt%) was significantly lower than in the case of sisal and jute, which accounted for 12.6 and 11.2 wt%, respectively. Indeed, considering that hemicellulose and lignin constitute the major amorphous regions of lignocellulose, jute fibers exhibited the highest content of amorphous constituents (18.1 wt%), followed by sisal (17.6 wt%), and hemp (9.2 wt%). Jute and sisal exhibited a similar chemical composition, as the cellulose content accounted for 80.2 and 80.7 wt%, respectively, while cellulose in hemp fibers accounted for 90.0 wt%. Apparently, the chemical characteristics of jute and sisal are similar, which should lead to similar CNF characteristics. Indeed, the reported results in Table 4 support this hypothesis, as nanofibrillation yield and light transmittance of jute and sisal CNFs, regardless the oxidation degree and the HPH sequence, exhibited similar values, while the obtained results for hemp CNFs were significantly different, particularly at low oxidation degrees and HPH intensity. Nonetheless, as it will be later discussed, high oxidation degrees on sisal fibers also led to rod-like structures, as in the case of hemp, while this was not observed in the case of jute. Considering the definition above of recalcitrance, the features influencing relative recalcitrance of biomass might be, among others, the chemical complexity and crystallinity (Zhao et al., 2012). On the one hand, the higher presence of lignin in jute might have a direct impact on the TEMPO-mediated oxidation performance, where part of the oxidizer is consumed by lignin rather than cellulose. On the other, the access of the oxidizer to more crystalline structures may be difficult due to steric effects. The quantification of recalcitrance is somewhat still under investigation that surely requires further research, with well-designed factorial plans to successfully parameterize its effect and influence over the performance of different treatments to biomass (Kruer-Zerhusen et al., 2018).

One of the key parameters for monitoring the evolution of CNFs properties is cationic demand (Serra-Parareda et al., 2021). Indeed, cationic demand has been reported to perfectly correlate with other characteristics (i.e. nanofibrillation yield, surface area), rather than other properties such as water retention value, mainly due to the chemical changes that CNFs may experience during HPH (Qua et al., 2011; Gu et al., 2018). Cationic demand has been reported to provide an indication of the surface area of CNFs, which may be estimated by the monolayer adsorption of polyDADMAC, used for the back titration process of this determination (Espinosa et al., 2016). As detailed in the previous section, cationic demand was determined using a high-molecular weight (Mw) polyDADMAC, as it may have an effect on the determination on this parameter. Briefly, low-Mw polyDADMAC, ranging between 7.5 and 15 kDa, may penetrate into the CNFs structure, obtaining the total CNF charge. On the other hand, high-Mw polyDADMAC, namely above 100 kDa, results in a lower charge, as only surface charge is neutralized (Zhang et al., 2016). Fig. 3 shows the obtained cationic demands as function of the fiber source, oxidation degree, and HPH sequence.

Apparently, the effect of HPH was lower in those fibers oxidized at 5 mmol/g than those at 15 mmol/g, as no significant enhancement was found as the HPH process was intensified. In addition, no significant differences were found between the three fiber sources. In all cases, hemp CNFs exhibited the lowest cationic demand, while jute obtained the highest values. The lower values of cationic demand of hemp may be attributed to the abovementioned chemical differences between the selected fiber sources, as hemicellulose has been reported to promote fibrillation (Chaker et al., 2013; Tarrés et al., 2017b).

Assuming that polyDADMAC adsorption occurs by means of two different mechanisms, namely (i) ionic interaction between carboxyl groups and the polymer, and (ii) hydrogen bonding and Van der Waals forces, and that its adsorption can be assumed in the form of a monolayer, the surface area of CNFs can be calculated considering the surface area of polyDADMAC. Considering that the polyDADMAC chain exhibits a cylindrical geometry, the surface area of this cationic polymer can be estimated into $4.87 \cdot 10^{17}$ $nm^2/\mu eq$ (Tarrés et al., 2017a). Further, the obtained values of cationic demand and carboxyl content are useful to calculate the CNFs' theoretical surface area (Eq. 4).

$$SSA_{CNF} = (CD - CC) \cdot SSA_{polyDADMAC} \quad (4)$$

where SSA_{CNF} (nm^2/g) and $SSA_{polyDADMAC}$ ($nm^2/\mu eq$) are the specific surface area of CNFs and polyDADMAC, respectively. Finally, assuming that CNFs are perfect cylinders, and that cellulose density is 1.5 g/cm^3, average diameter can be estimated (Table 5).

The lower SSA of those CNFs prepared from hemp, clearly indicate that the extent of fibrillation was lower. Indeed, this is in agreement with the above discussion on the possibility of generating rod-like structures, similar to CNCs, when hemp fibers are subjected to TEMPO-mediated oxidation and HPH. As expected, the highest SSA was found in jute CNFs, particularly for those fibers with a high oxidation degree and HPH intensity (310 m^2/g), leading to the lowest diameter. The obtained values of SSA were in accordance with previously reported values for other raw materials, such as eucalyptus or pine (Tarrés et al., 2019). However, at low oxidation degree, hemp exhibited a slightly lower SSA, confirming the generation of more rigid structures with

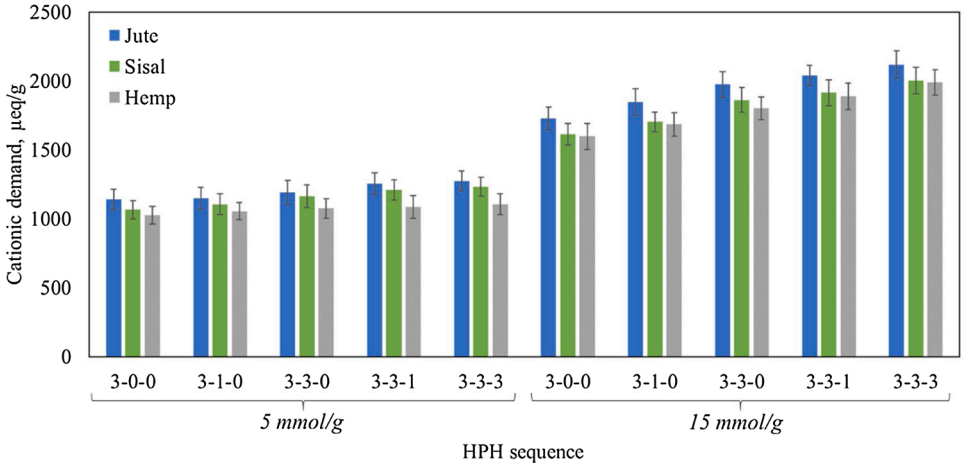

Fig. 3. Cationic demand of the obtained CNFs as function of the oxidation degree and HPH sequence.

Table 5
Estimated specific surface area (SSA) and average diameter (d) of the obtained CNFs as function of the fiber source, oxidation degree and HPH sequence.

OA (mmol/g)	HPH sequence	SSA (m^2/g)			d (nm)		
		Jute	Sisal	Hemp	Jute	Sisal	Hemp
5	3-0-0	174	134	109	15	19	23
	3-1-0	177	154	123	15	16	20
	3-3-0	197	182	132	14	14	19
	3-3-1	229	204	138	12	12	18
	3-3-3	238	216	148	11	12	17
15	3-0-0	119	118	115	21	21	22
	3-1-0	178	162	157	15	15	16
	3-3-0	240	240	213	10	10	12
	3-3-1	271	264	255	9	10	10
	3-3-3	310	309	306	8	8	8

lower surface than in the case of the other tested raw materials. Further, the obtained values were significantly higher than others reported for lignin-containing CNFs, both from wood and non-wood resources (Rojo et al., 2015; Espinosa et al., 2016).

Apparently, apart from impacting the diameter, TEMPO-mediated oxidation and HPH had a significant impact on fiber length, leading to a remarkable decrease on the slenderness or aspect ratio (Fig. 4).

The morphological characteristics observed in Fig. 2 were confirmed by the analysis of the aspect ratio (Fig. 4). While no significant differences were found for those CNFs oxidized with 5 mmol/g, although sisal accounted for the lowest aspect ratio in all cases, the effect of HPH was significant for CNFs produced from the oxidative process at 15 mmol/g of NaClO. Indeed, jute CNFs exhibited high aspect ratios compared to those produced from sisal and hemp, which accounted for values comprised between 4 and 6. Further, CNFs prepared from sisal at 15 mmol/g and HPH sequences of 3-3-0, 3-3-1 and 3-3-3 were found to be colloidally stable in water and, thus, aspect ratio was not obtained by means of the gel point determination. This supports the hypothesis of the presence of CNCs in the sisal and hemp fibers at high oxidation and HPH degree, rather than CNFs (Winter et al., 2010; Moberg et al., 2017; Isogai and Zhou, 2019). This might be caused by the inherent differences on the starting material, both in morphological and chemical terms, as it has been previously reported. Indeed, depending on the starting material, different CNF/CNCs characteristics might be obtained for certain reaction and fibrillation conditions (Salminen et al., 2017; Zhou et al., 2018). This is particularly interesting, since mass production at industrial level could be easily performed merely adjusting the oxidation conditions, which provides versatility to the process, with no need of having two different production lines for CNFs and CNCs.

The rheological behavior of CNF and CNC suspensions is a complex system influenced by the aspect ratio, the specific surface area, and the interactions between the nanofibers themselves (Koponen, 2020). As described in the previous section, the shear-thinning behavior was assessed by means of viscosimetric analysis of CNF and CNC suspensions at 1 wt% through the Ostwald de Waele equation, leading to the consistency factor (K) and flow behavior index (n). Results are shown in Table 6, and the evolution of the apparent viscosity as function of the shear rate with the correlation factor R^2, in Fig. S2 and Table S1.

As expected, jute CNFs exhibited an absolutely different rheological behavior than those made from sisal or hemp. According to the obtained aspect ratios from the gel point determination, CNFs prepared from jute exhibited the highest slenderness. In addition, from the TEM observation, it was confirmed that, at certain oxidation degree, the surface fibrillation was more pronounced than in the case of hemp or sisal CNFs. It is well known that Power-law fluids can be subdivided into three different categories, depending on the flow behavior index. Fluids exhibiting n values below the unity, are categorized as shear thinning fluids, while higher n lead to Newtonian ($n = 1$) and dilatant ($n > 1$) fluids (Filipova et al., 2020). Thus, the obtained CNF suspensions clearly exhibited a shear thinning behavior, although some differences were found depending on the fiber source, the oxidation degree and the HPH sequence. Indeed, shear thinning was apparent in all cases except for those CNFs prepared from hemp and oxidized with an OA of 15 mmol/g, where the decrease of the apparent viscosity (η) was moderate at increasing shear rates. This can be attributed to the low aspect ratio of the obtained CNFs, as well as the generation of rod-like nanostructures, similar to CNCs, as discussed above. Images of the obtained CNFs suspensions at 1 wt% consistency at different oxidation degree and HPH

Table 6
Consistency factor (K) and flow behavior index (n) as function of the fiber source, oxidation degree and HPH sequence.

OA (mmol/g)	HPH sequence	Consistency factor (K)			Flow behavior index (n)		
		Jute	Sisal	Hemp	Jute	Sisal	Hemp
5	3-0-0	13.2	1.8	2.2	0.33	0.40	0.42
	3-1-0	17.1	7.4	5.6	0.35	0.34	0.39
	3-3-0	41.8	17.3	10.9	0.28	0.32	0.33
	3-3-1	47.6	22.3	14.1	0.27	0.29	0.33
	3-3-3	48.6	23.1	19.6	0.19	0.29	0.31
15	3-0-0	24.1	4.6	0.12	0.25	0.38	0.60
	3-1-0	28.9	14.4	0.10	0.27	0.36	0.68
	3-3-0	26.1	3.3	0.07	0.26	0.36	0.76
	3-3-1	20.4	1.2	0.06	0.27	0.45	0.75
	3-3-3	8.6	0.8	0.05	0.30	0.56	0.77

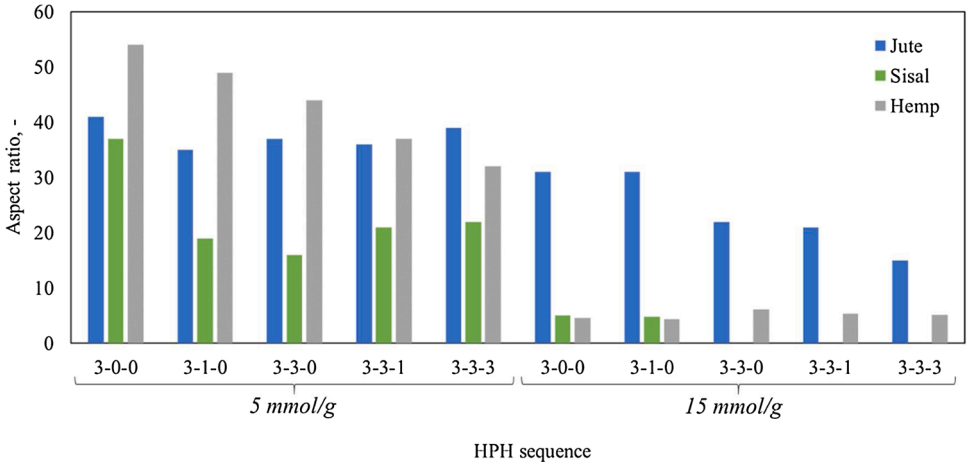

Fig. 4. Aspect ratio of the obtained CNFs as function of the oxidation degree and HPH sequence.

intensity are shown in Fig. S3.

Focusing on the consistency factor (K), it becomes apparent that those CNFs prepared with an OA of 5 mmol/g, regardless the fiber source, exhibited an increasing *K* with the HPH sequence. Concretely, jute CNFs exhibited a significantly higher *K* than sisal or hemp CNFs, which is in line with the above discussion on the morphological characteristics of CNFs. This higher *K* brings to the light the higher capacity of jute CNFs to create an entangled network, leading to thicker gels than sisal or hemp CNFs. In addition, this is supported by the flow behavior index, where the lowest values were found precisely for jute CNFs regardless the HPH sequence, although a decreasing tendency of *n* was found for all the fiber sources. These lower *n* values, together with the higher *K*, for jute CNFs clearly indicate the higher viscosity and non-Newtonian characteristics of jute CNFs, provided by the surface fibrillation and morphological characteristics. It must be mentioned that *K* is strongly related to the solids content of the suspension, which was set at 1 wt%. Previous results indicate that at increasing solids content, consistency factor increases, while the flow behavior remained constant (Nazari et al., 2016).

Nonetheless, the rheological assessment gains interest for those CNFs prepared from fibers oxidized at 15 mmol/g of OA. At certain point of the HPH process, jute and sisal CNFs experienced a breakage of the gel structure, while in the case of hemp, this effect was observed from the very beginning of the HPH process. Concretely, the *K* of jute CNFs dropped from 20.4–8.6 when they were subjected to two additional passes at 900 bar (from 3-3-1 to 3-3-3). This effect was also noticed with an increase on the *n*, from 0.27 to 0.30. In the case of sisal CNFs, this gel breakage was observed at lower HPH intensity, as the *K* decreased from 14.36 to 3.28 when two additional cycles at 600 bar were applied to the CNF suspension (from 3-1-0 to 3-3-0), which was also observed in the increase on the *n*. In addition, *K* decreased as HPH was intensified (from 3.3 to 0.8 for HPH sequences of 3-3-0 to 3-3-3, respectively), while *n* followed an increasing tendency, achieving a value of 0.56 at 3-3-3. The premature gel breakage of sisal CNFs compared to jute is supported by the lower *K* values of sisal CNFs oxidized with 5 mmol/g of OA. In the case of hemp fibers, it was found that gel was broken from the very beginning of the HPH process, as low values were found for *K,* while *n* accounted for significantly higher values than the rest of fiber sources, approaching a value of 1, where Newtonian fluids are found. This behavior is interesting for applications such as drilling fluids, as hemp nanostructures could serve as thickener due to their high concentration of carboxylate groups, as well as the low shear-thinning effect (Li et al., 2016). In addition, they may play a key role on the development of nanocellulose-based coatings for paper, as viscosity is a limiting aspect, particularly in low-basis weight papers. Indeed, the high surface area of hemp CNFs, together with their apparently rod-like structure, would lead to successful surface coverage while maintaining the viscosity at moderate levels, which may contribute to the increase of the solid content of other coating constituents (Hubbe et al., 2017; Liu et al., 2017). The highly charged surface of the obtained CNFs and CNCs may limit their entanglement capacity, as repulsion forces may contribute to the disaggregation of floccules generated at lower oxidation degree. This might be occurring because the studied suspensions are based on CNF/CNC-water systems, while depletion interactions might be found when they are incorporated into other polymers and might be considered in terms of their rheological behavior (Souza et al., 2019).

TEMPO-oxidized CNFs have been reported to provide a strong and entangled network in the form of aqueous suspensions. This has been even confirmed by several authors and, in principle, no significant effects of the raw material characteristics have been observed on the rheological properties. Here, considering the low recalcitrance of the selected raw materials, as they come from non-woody resources, the hypothesis related to the effects of the raw material characteristics on the rheological properties, glimpsed by Nechyporchuk et al. (2014), is confirmed. Although the obtained suspensions clearly exhibited a shear-thinning behavior, the obtained consistency factors are far from those reported in the literature for CNF suspensions, even those not produced by means of TEMPO-mediated oxidation. This could be attributed to the significant differences on the obtained morphologies, as some of the cellulosic nanostructures may be categorized as CNCs and some others as CNFs. These differences were confirmed by means of determining the 2D fractal dimension (D_2) of the obtained nanostructures, which is a useful parameter for estimating the irregularity or the roughness of ideal fractals and natural objects not corresponding to classical geometries. While acquisition of diameter and length values can be performed in a simple and direct way in rod-like particles as those of CNC samples, it becomes a challenge when one is dealing with CNFs. On the one hand, the use of a classical diameter distribution may provide higher importance to small branches and fibrils than to macroscopic fibers and could hind important information on how nanofibrils are distributed in a matrix. On the other hand, CNF length cannot be more than estimated but without a manner to prove that the estimation is correct. Thus, we have attended to the fractal dimension parameter, which is a measurement of the complexity of an object and has been recognized as a very useful tool for estimating the irregularity or the roughness of ideal fractals and natural objects which are not included in classical geometry. With this parameter, one could obtain relevant information on how the fibrils are distributed in a sample, i.e. a network of nanofibrils with a homogeneous diameter, a thick fiber with thousands of branches or some individualized particles with the shape of rods (CNCs), and could allow to gain insight into the rheological behavior. Although there are methods that aim to estimate the 3D fractal dimension of objects, they are limited to microparticles, while the estimation of 3D fractal dimension of nanoparticles is still challenging. Thus, many authors have resorted to the quantification of a projected fractal dimension in 2D through image analysis (Campano et al., 2021).

D_2 was determined for all the tested samples and correlated with the consistency factor (K) and the flow behavior index (n), as it can be observed in Fig. 5. Disaggregated data, by raw material, is provided in Figs. S4, S5 and S6 from the supplementary material. The direction of the arrows indicates the order of the HPH sequences.

Interestingly, data could be grouped in two different groups, corresponding to those structures with D_2 comprised between 1.20 and 1.40, approximately, and those accounting for D2 values above 1.50. The first group, considered as CNCs, exhibited higher values of flow behavior index and lower consistency factors. This indicates that the resulting suspensions were less shear-thinning, approaching a Newtonian behavior, and exhibited moderate viscosity in a wide range of shear rates. In nanostructured cellulose, the value of D_2 is influenced by the complexity of the structures (i.e. extent of surface fibrillation, entanglement with adjacent structures, flexibility) and the diameter of a single nanostructure. Only two types of structures were included in the first group (hemp and sisal, both oxidized at 15 mmol/g OA) and both exhibited decreasing consistency factor and increasing flow behavior index as HPH was intensified. However, while D_2 significantly decreased for the case of hemp CNCs, no apparent changes were observed in the case of sisal CNCs. This could be attributed to the morphological differences observed in Figs. 2 and S1, as length apparently decreased in the case of hemp, while no apparent morphological changes are observed in the case of sisal as HPH advances. However, cationic demand of those CNCs prepared from sisal oxidized with 15 mmol/g experienced a significant enhancement as HPH was intensified, which may contribute to an increase of the repulsive forces between CNCs and, thus, preventing the formation of aggregates (Souza et al., 2019). In this first group, highly fibrillated sisal oxidized at 5 mmol/g (HPH sequence of 3-3-3) was also found. This might be attributed to the generation of CNCs after the whole HPH sequence, while CNFs might be also present in the suspension. This can be observed in Fig. 2.

Regarding the second group ($D_2 > 1.50$), identified as CNFs and corresponding to the rest of samples, D_2 appeared to be more heterogeneous, while slight changes were observed in the flow behavior index and the consistency factor, except for some specific cases such as those

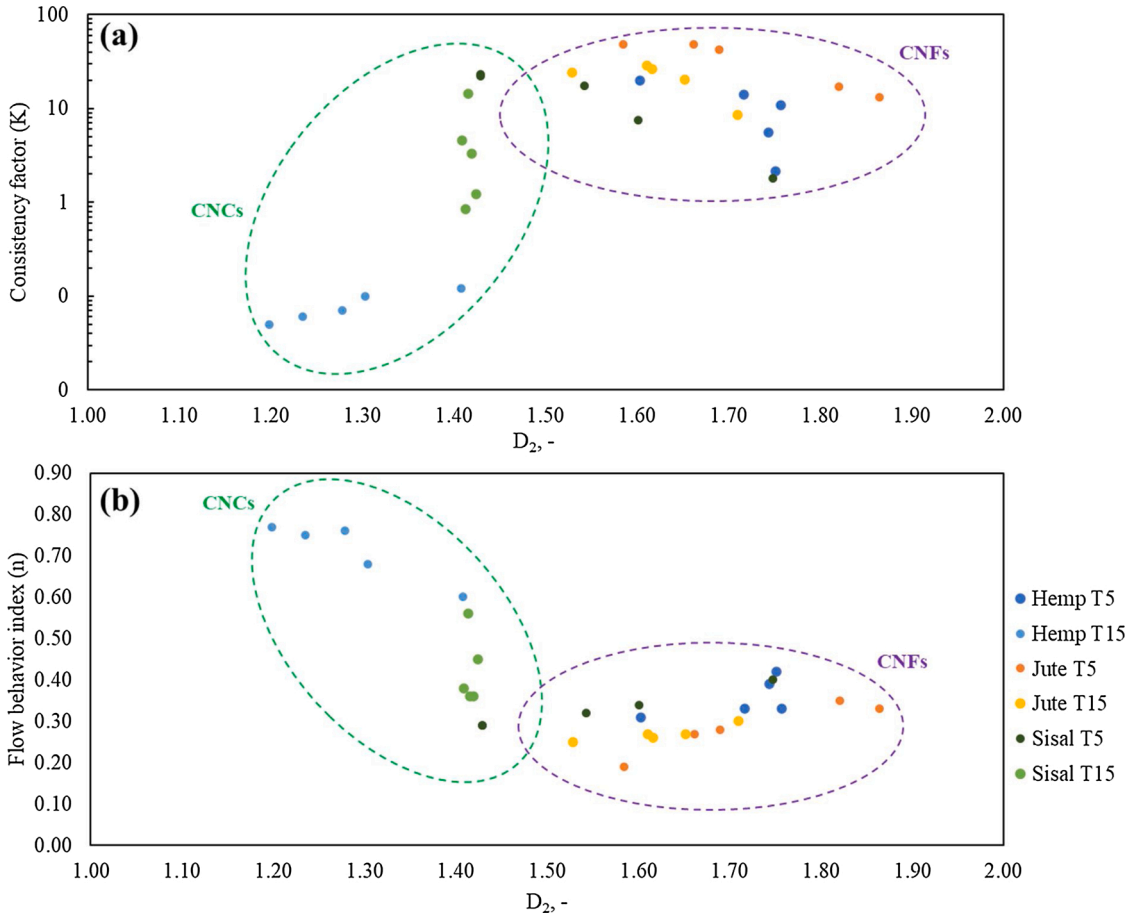

Fig. 5. Correlation between 2D fractal dimension (D2) and (a) consistency factor, and (b) flow behavior index.

CNFs prepared from hemp and sisal, both oxidized at 5 mmol/g. In all cases, except for jute oxidized at 15 mmol/g, the HPH process led to a reduction in the D_2, which indicates a reduction on the diameter, increase of the repulsion forces and, thus, disentanglement of the cellulosic nanostructures (Figs. S4, S5 and S6). Those fibers oxidized at 5 mmol/g experienced an increase on their shear-thinning behavior, exhibiting a decrease on their flow behavior index and an increase on their consistency factor. This indicates that while diameter was decreased and disentanglement promoted, surface area was increased, leading to a higher water absorption capacity and, thus, an absolute increase on suspension viscosity (Hubbe et al., 2017; Gu et al., 2018). The case of jute is of particular interest, as D2 appeared to increase with HPH, as well as the flow behavior index and, thus, leading to a reduction on the consistency factor. This might be attributed to the higher lignin content of jute, which may have a negative effect on the effectiveness of the oxidative process, as well as to the differences on the crystallinity and, apparently, crystal size (Zhou et al., 2018; Jiang et al., 2020). The obtained results bring to the light the suitability of some non-woody plants to be used as raw material for CNC production by means of TEMPO-mediated oxidation, which contributes to their valorization and is advantageous for mass production at industrial level compared to acid-based treatments such as hydrolysis (Zhou et al., 2018).

Overall, the obtained results from the assessment of the rheological behavior confirm the morphological characteristics detailed above, bringing to the light the influence of the raw material on the resulting properties of CNF/CNCs. Further, it appears that hemp CNFs could have potential opportunities in several sectors, particularly in those where the CNF suspension needs to be pumped, reducing the risk of cavitation.

4. Conclusions

The present work shows the initial, intermediate, and final characteristics of non-woody cellulose nanofibers made of jute, sisal, and hemp by means of TEMPO-mediated oxidation and high-pressure homogenization. Jute has been found to provide similar characteristics to CNFs prepared from some wood resources (i.e. eucalyptus wood), as the resulting CNFs exhibited fibrillar structures. This has been attributed to the initial chemical and morphological characteristics of jute, as it was the one presenting a higher presence of amorphous constituents (hemicellulose and lignin), although the crystallinity index was the highest. Contrarily, sisal and hemp fibers have apparently led to rod-like structures, indicating that at a high intensity of HPH, particularly for those oxidized with 15 mmol/g of NaClO, CNCs were obtained rather than CNFs. The presence of CNC-like structures has been corroborated by means of TEM observation, gel point assessment, and the rheological studies, where gel breakage was found at certain level of fibrillation with a clear decrease of the consistency factor. In addition, the flow behavior index of hemp nanostructures indicated that the suspension experienced a low shear-thinning behavior with a clear tendency to approach Newtonian fluids. Fractal dimension in 2D (D_2) has been used to correlate the obtained rheological characteristics, which indicates that highly complex structures ($D_2 > 1.50$) exhibited an increasing shear-thinning behavior and morphologies similar to CNFs, while at moderately complex structures ($1.20 < D_2 < 1.40$) the rheological behavior tended to Newtonian fluids, as the obtained particles exhibited a rod-like structure typical from CNCs. This rheological behavior was significantly different to those cellulose nanostructures obtained by means of TEMPO-mediated oxidation from wood, which has been attributed to the lower recalcitrance of non-woody plants. In addition, the higher

recalcitrance of jute has been proposed compared to sisal and hemp, which may explain the differences on the resulting characteristics of CNFs/CNCs. Nonetheless, this is an outstanding concept that requires further research in terms of structure, chemical composition, and physical features. These characteristics open a wide range of opportunities to such CNFs/CNCs, as they might be easily transported (avoiding pump cavitation) and might impart low effects on the rheology of other suspensions while maintaining the intrinsic characteristics of nanocellulose. Overall, the present work shows the feasibility of using annual plants (jute, sisal, and hemp) as potential raw material for TEMPO-mediated oxidized nanocellulose, which may constitute a strong alternative to wood-based CNFs, as both CNFs and CNCs could be easily obtained by means of adjusting the oxidation intensity.

CRediT authorship contribution statement

Ferran Serra-Parareda: Investigation and Methodology **Quim Tarrés:** Investigation, data curation,and Writing – original draft**, José Luis Sanchez-Salvador:** Investigation, Methodology and data curation**, Cristina Campano:** Investigation, methodology, formal análisis, and writing-review**, M. Àngels Pèlach:** Resources and project administration**, Pere Mutjé:** Supervision, resources, project administration, and writing-review**, Carlos Negro:** Supervision, resources, project administration, and writing-review**, Marc Delgado-Aguilar:** Supervision, validation, Writing – original draft, Writing – review & editing.

Declaration of Competing Interest

The authors declare that they have no known competing financial interests or personal relationships that could have appeared to influence the work reported in this paper.

Acknowledgments

The authors want to acknowledge the Spanish Ministry of Economy and Competitiveness for the funding of the project NANOPROSOST, references CTQ2017-85654-C2-1-R and CTQ2017-85654-C2-2-R. Authors want also to thank Spanish Ministry of Science and Innovation for the Juan de la Cierva aid of Cristina Campano (Ref. FJC2019-040298-I), the support of Universidad Complutense de Madrid and Banco de Santander for the grant of J.L. Sanchez-Salvador (CT17/17) and the Spanish National Centre of Electronic Microscopy for the support during image acquisition. Marc Delgado-Aguilar is a Serra Húnter Fellow.

Appendix A. Supplementary data

Supplementary material related to this article can be found, in the online version, at doi:https://doi.org/10.1016/j.indcrop.2021.113877.

References

Abd El-Sayed, E.S., El-Sakhawy, M., El-Sakhawy, M.A.M., 2020. Non-wood fibers as raw material for pulp and paper industry. Nord Pulp Pap Res. J. 35, 215–230. https://doi.org/10.1515/npprj-2019-0064.

Abdul Khalil, H.P.S., Davoudpour, Y., Islam, M.N., et al., 2014. Production and modification of nanofibrillated cellulose using various mechanical processes: a review. Carbohydr. Polym. 99, 649–665. https://doi.org/10.1016/j.carbpol.2013.08.069.

Alila, S., Besbes, I., Vilar, M.R., et al., 2013. Non-woody plants as raw materials for production of microfibrillated cellulose (MFC): a comparative study. Non-woody plants as raw materials for production of microfibrillated cellulose (MFC): a comparative study. Ind. Crops Prod. 41, 250–259. https://doi.org/10.1016/j.indcrop.2012.04.028.

Ankerfors, M., Duker, E., Lindström, T., 2013. Topo-chemical modification of fibres by grafting of carboxymethyl cellulose in pilot scale. Nord Pulp Pap Res J 28, 6–14.

Besbes, I., Alila, S., Boufi, S., 2011. Nanofibrillated cellulose from TEMPO-oxidized eucalyptus fibres: effect of the carboxyl content. Carbohydr. Polym. 84, 975–983. https://doi.org/10.1016/j.carbpol.2010.12.052.

Blanco, A., Monte, M.C., Campano, C., et al., 2018. Nanocellulose for industrial use: cellulose nanofibers (CNF), cellulose nanocrystals (CNC), and bacterial cellulose (BC). Handbook of Nanomaterials for Industrial Applications. Micro and Nano Technologies, pp. 74–126.

Bondeson, D., Mathew, A., Oksman, K., 2006. Optimization of the isolation of nanocrystals from microcrystalline cellulose by acid hydrolysis. Cellulose 13, 171–180. https://doi.org/10.1007/s10570-006-9061-4.

Boufi, S., González, I., Delgado-Aguilar, M., et al., 2016. Nanofibrillated cellulose as an additive in papermaking process: a review. nanofibrillated cellulose as an additive in papermaking process: a review. Carbohydr. Polym. 154, 151–166. https://doi.org/10.1016/j.carbpol.2016.07.117.

Campano, C., Balea, A., Blanco, Á., Negro, C., 2020. A reproducible method to characterize the bulk morphology of cellulose nanocrystals and nanofibers by transmission electron microscopy. Cellulose 27, 4871–4887. https://doi.org/10.1007/s10570-020-03138-1.

Campano, C., Lopez-Exposito, P., Gonzalez-Aguilera, L., et al., 2021. In-depth characterization of the aggregation state of cellulose nanocrystals through analysis of transmission electron microscopy images. In-depth characterization of the aggregation state of cellulose nanocrystals through analysis of transmission electron microscopy images. Carbohydr. Polym. 254, 117271 https://doi.org/10.1016/j.carbpol.2020.117271.

Cao, X., Ding, B., Yu, J., Al-Deyab, S.S., 2013. In situ growth of silver nanoparticles on TEMPO-oxidized jute fibers by microwave heating. Carbohydr. Polym. 92, 571–576. https://doi.org/10.1016/j.carbpol.2012.08.091.

Chaker, A., Alila, S., Mutjé, P., et al., 2013. Key role of the hemicellulose content and the cell morphology on the nanofibrillation effectiveness of cellulose pulps. Cellulose. https://doi.org/10.1007/s10570-013-0036-y.

Chokshi, S., Parmar, V., Gohil, P., Chaudhary, V., 2020. Chemical composition and mechanical properties of natural fibers. J Nat Fibers 00, 1–12. https://doi.org/10.1080/15440478.2020.1848738.

De France, K.J., Hoare, T., Cranston, E.D., 2017. Review of hydrogels and aerogels containing nanocellulose. Chem. Mater. 29, 4609–4631. https://doi.org/10.1021/acs.chemmater.7b00531.

Deepa, B., Abraham, E., Cherian, B.M., et al., 2011. Structure, morphology and thermal characteristics of banana nano fibers obtained by steam explosion. Structure, morphology and thermal characteristics of banana nano fibers obtained by steam explosion. Bioresour. Technol. 102, 1988–1997. https://doi.org/10.1016/j.biortech.2010.09.030.

Domínguez-Robles, J., Tarrés, Q., Delgado-Aguilar, M., et al., 2018. Approaching a new generation of fiberboards taking advantage of self lignin as green adhesive. Int. J. Biol. Macromol. https://doi.org/10.1016/j.ijbiomac.2017.11.005.

Dufresne, A., 2018. Cellulose nanomaterials as green nanoreinforcements for polymer nanocomposites. Philos. Trans. R. Soc. A Math. Phys. Eng. Sci. 376.

Duker, E., Ankertors, M., Lindström, T., Nordmark, G.G., 2008. The use of CMC as a dry strength agent - the interplay between CMC attachment and drying. Nord Pulp Pap Res J 23, 65–71.

Ebringerová, A., Heinze, T., 2000. Xylan and xylan derivatives - Biopolymers with valuable properties, 1: naturally occurring xylans structures, isolation procedures and properties. Macromol. Rapid Commun. 21, 542–556. https://doi.org/10.1002/1521-3927(20000601)21:9<542::AID-MARC542>3.0.CO;2-7.

Ek, M., Gellerstedt, G., Henriksson, G., 2017. Pulp and Paper Chemistry and Technology, Vol. 2.

Espinosa, E., Tarrés, Q., Delgado-Aguilar, M., et al., 2016. Suitability of wheat straw semichemical pulp for the fabrication of lignocellulosic nanofibres and their application to papermaking slurries. Suitability of wheat straw semichemical pulp for the fabrication of lignocellulosic nanofibres and their application to papermaking slurries. Cellulose 23, 837–852. https://doi.org/10.1007/s10570-015-0807-8.

Favier, V., Canova, G.R., Shrivastava, S.C., Cavaillé, J.Y., 1997. Mechanical percolation in cellulose whisker nanocomposites. Polym Eng Sci 37, 1732–1739.

Filipova, I., Serra, F., Tarrés, Q., et al., 2020. Oxidative treatments for cellulose nanofibers production: a comparative study between TEMPO-mediated and ammonium persulfate oxidation. Oxidative treatments for cellulose nanofibers production: a comparative study between TEMPO-mediated and ammonium persulfate oxidation. Cellulose 27, 10671–10688. https://doi.org/10.1007/s10570-020-03089-7.

Fujisawa, S., Okita, Y., Fukuzumi, H., et al., 2011. Preparation and characterization of TEMPO-oxidized cellulose nanofibril films with free carboxyl groups. Preparation and characterization of TEMPO-oxidized cellulose nanofibril films with free carboxyl groups. Carbohydr. Polym. 84, 579–583. https://doi.org/10.1016/j.carbpol.2010.12.029.

Gon, D., Das, K., Paul, P., Maity, S., 2013. Jute composites as wood substitute. Int. J. Text Sci. 1, 84–93. https://doi.org/10.5923/j.textile.20120106.05.

Gontard, N., Sonesson, U., Birkved, M., et al., 2018. A research challenge vision regarding management of agricultural waste in a circular bio-based economy A research challenge vision regarding management of agricultural waste in a circular bio-based economy. Crit. Rev. Environ. Sci. Technol. 48, 614–654. https://doi.org/10.1080/10643389.2018.1471957.

Gorur, Y.C., Larsson, P.A., Wågberg, L., 2020. Self-fibrillating cellulose fibers: rapid in situ nanofibrillation to prepare strong, transparent, and gas barrier nanopapers. Biomacromolecules 21, 1480–1488. https://doi.org/10.1021/acs.biomac.0c00040.

Gu, F., Wang, W., Cai, Z., et al., 2018. Water retention value for characterizing fibrillation degree of cellulosic fibers at micro and nanometer scales. Water retention value for characterizing fibrillation degree of cellulosic fibers at micro and nanometer scales. Cellulose 25, 2861–2871. https://doi.org/10.1007/s10570-018-1765-8.

Habibi, Y., Lucia, L.A., Rojas, O.J., 2010. Cellulose nanocrystals : chemistry. Self-Assembly, and Applications. d 3479–3500. https://doi.org/10.1021/cr900339w.

Henriksson, M., Henriksson, G., Berglund, L.A., Lindström, T., 2007. An environmentally friendly method for enzyme-assisted preparation of microfibrillated cellulose (MFC) nanofibers. Eur. Polym. J. 43, 3434–3441. https://doi.org/10.1016/j.eurpolymj.2007.05.038.

Hubbe, M.A., 2014. Prospects for maintaining strength of paper and paperboard products while using less forest resources: a review. BioResources 9, 1634–1763.

Hubbe, M.A., Tayeb, P., Joyce, M., et al., 2017. Rheology of nanocellulose-rich aqueous suspensions: a review. rheology of nanocellulose-rich aqueous suspensions: a review. BioResources 12, 9556–9661. https://doi.org/10.15376/biores.12.4.Hubbe.

Iguchi, M., Yamanaka, S., Budhiono, A., 2000. Bacterial cellulose - a masterpiece of nature's arts. J. Mater. Sci. 35, 261–270. https://doi.org/10.1023/A.

Isogai, A., Saito, T., Fukuzumi, H., 2011. TEMPO-oxidized cellulose nanofibers. Nanoscale 3, 71–85. https://doi.org/10.1039/c0nr00583e.

Isogai, A., Zhou, Y., 2019. Diverse nanocelluloses prepared from TEMPO-oxidized wood cellulose fibers: nanonetworks, nanofibers, and nanocrystals. Curr. Opin. Solid State Mater. Sci. 23, 101–106. https://doi.org/10.1016/j.cossms.2019.01.001.

Jiang, J., Chen, H., Liu, L., et al., 2020. Influence of chemical and enzymatic TEMPO-Mediated oxidation on chemical structure and nanofibrillation of lignocellulose influence of chemical and enzymatic TEMPO-Mediated oxidation on chemical structure and nanofibrillation of lignocellulose. ACS Sustain. Chem. Eng. 8, 14198–14206. https://doi.org/10.1021/acssuschemeng.0c05291.

Kekäläinen, K., Liimatainen, H., Illikainen, M., et al., 2014. The role of hornification in the disintegration behaviour of TEMPO-oxidized bleached hardwood fibres in a high-shear homogenizer. The role of hornification in the disintegration behaviour of TEMPO-oxidized bleached hardwood fibres in a high-shear homogenizer. Cellulose 21, 1163–1174. https://doi.org/10.1007/s10570-014-0210-x.

Koponen, A.I., 2020. The effect of consistency on the shear rheology of aqueous suspensions of cellulose micro- and nanofibrils: a review. Cellulose 27, 1879–1897. https://doi.org/10.1007/s10570-019-02908-w.

Kruer-Zerhusen, N., Cantero-Tubilla, B., Wilson, D.B., 2018. Characterization of cellulose crystallinity after enzymatic treatment using Fourier transform infrared spectroscopy (FTIR). Cellulose 25, 37–48. https://doi.org/10.1007/s10570-017-1542-0.

Lasseuguette, E., Roux, D., Nishiyama, Y., 2008. Rheological properties of microfibrillar suspension of TEMPO-oxidized pulp. Cellulose 15, 425–433. https://doi.org/10.1007/s10570-007-9184-2.

Levanič, J., Šenk, V.P., Nadrah, P., et al., 2020. Analyzing TEMPO-Oxidized cellulose Fiber morphology: new insights into optimization of the oxidation process and nanocellulose dispersion quality. analyzing TEMPO-Oxidized cellulose Fiber morphology: new insights into optimization of the oxidation process and nanocellulose dispersion quality. ACS Sustain. Chem. Eng. 8, 17752–17762. https://doi.org/10.1021/acssuschemeng.0c05989.

Li, M.C., Wu, Q., Song, K., et al., 2016. Cellulose nanocrystals and polyanionic cellulose as additives in bentonite water-based drilling fluids: rheological modeling and filtration mechanisms. cellulose nanocrystals and polyanionic cellulose as additives in bentonite water-based drilling fluids: rheological modeling and filtration mechanisms. Ind. Eng. Chem. Res. 55, 133–143. https://doi.org/10.1021/acs.iecr.5b03510.

Lin, X., Wu, Z., Zhang, C., et al., 2018. Enzymatic pulping of lignocellulosic biomass. Enzymatic pulping of lignocellulosic biomass. Ind. Crops Prod. 120, 16–24. https://doi.org/10.1016/j.indcrop.2018.04.033.

Liu, C., Du, H., Dong, L., et al., 2017. Properties of nanocelluloses and their application as rheology modifier in paper coating. properties of nanocelluloses and their application as rheology modifier in paper coating. Ind. Eng. Chem. Res. 56, 8264–8273. https://doi.org/10.1021/acs.iecr.7b01804.

Loranger, E., Piché, A.-O., Daneault, C., 2012. Influence of high shear dispersion on the production of cellulose nanofibers by ultrasound-assisted TEMPO-Oxidation of kraft pulp. Nanomaterials 2, 286–297. https://doi.org/10.3390/nano2030286.

Ludueña, L.N., Vecchio, A., Stefani, P.M., Alvarez, V.A., 2013. Extraction of cellulose nanowhiskers from natural fibers and agricultural byproducts. Fibers Polym 14, 1118–1127. https://doi.org/10.1007/s12221-013-1118-z.

Marques, G., Rencoret, J., Gutiérrez, A., del Río, J.C., 2010. Evaluation of the chemical composition of different non-woody plant fibers used for pulp and paper manufacturing. Open Agric J 4, 93–101. https://doi.org/10.2174/1874331501004010093.

Marques, G., Rencoret, J., Gutiérrez, A., del Río, J.C., 2014. Evaluation of the chemical composition of different non-woody plant fibers used for pulp and paper manufacturing. Open Agric. J. 4, 93–101. https://doi.org/10.2174/1874331501004010093.

Martinez, D.M., Buckley, K., Jivan, S., et al., 2001. Characterizing the mobility of papermaking fibres during sedimentation. Characterizing the mobility of papermaking fibres during sedimentation. 12th Fundam Res. Symp. 16, 225–254. https://doi.org/10.15376/frc.2001.1.225.CHARACTERIZING.

McCann, M.C., Carpita, N.C., 2015. Biomass recalcitrance: a multi-scale, multi-factor, and conversion-specific property. J. Exp. Bot. 66, 4109–4118. https://doi.org/10.1093/jxb/erv267.

Moberg, T., Sahlin, K., Yao, K., et al., 2017.) Rheological properties of nanocellulose suspensions: effects of fibril/particle dimensions and surface characteristics. Rheological properties of nanocellulose suspensions: effects of fibril/particle dimensions and surface characteristics. Cellulose 24, 2499–2510. https://doi.org/10.1007/s10570-017-1283-0.

Morales, L.O., Iakovlev, M., Martin-Sampedro, R., et al., 2014. Effects of residual lignin and heteropolysaccharides on the bioconversion of softwood lignocellulose nanofibrils obtained by SO2-ethanol-water fractionation. Effects of residual lignin and heteropolysaccharides on the bioconversion of softwood lignocellulose nanofibrils obtained by SO2-ethanol-water fractionation. Bioresour. Technol. 161, 55–62. https://doi.org/10.1016/j.biortech.2014.03.025.

Nascimento, D.Md., Almeida, J.S., Vale M do, S., et al., 2016. A comprehensive approach for obtaining cellulose nanocrystal from coconut fiber. Part I: proposition of technological pathways. Ind. Crops Prod. 93, 66–75. https://doi.org/10.1016/j.indcrop.2015.12.078.

Nazari, B., Kumar, V., Bousfield, D.W., Toivakka, M., 2016. Rheology of cellulose nanofibers suspensions: boundary driven flow. J Rheol (N Y N Y) 60, 1151–1159. https://doi.org/10.1122/1.4960336.

Nechyporchuk, O., Belgacem, M.N., Pignon, F., 2014. Rheological properties of micro-/nanofibrillated cellulose suspensions: wall-slip and shear banding phenomena. Carbohydr. Polym. 112, 432–439. https://doi.org/10.1016/j.carbpol.2014.05.092.

Okita, Y., Saito, T., Isogai, A., 2009. TEMPO-mediated oxidation of softwood thermomechanical pulp. Holzforschung 63, 529–535. https://doi.org/10.1515/HF.2009.096.

Oliaei, E., Lindén, P.A., Wu, Q., et al., 2020. Microfibrillated lignocellulose (MFLC) and nanopaper films from unbleached kraft softwood pulp microfibrillated lignocellulose (MFLC) and nanopaper films from unbleached kraft softwood pulp. Cellulose 27, 2325–2341. https://doi.org/10.1007/s10570-019-02934-8.

Oliver-Ortega, H., Julian, F., Espinach, F.X., et al., 2019. Research on the use of lignocellulosic fibers reinforced bio-polyamide 11 with composites for automotive parts: car door handle case study. Research on the use of lignocellulosic fibers reinforced bio-polyamide 11 with composites for automotive parts: car door handle case study. J. Clean. Prod. 226, 64–73. https://doi.org/10.1016/j.jclepro.2019.04.047.

Osong, S.H., Norgren, S., Engstrand, P., 2016. Processing of wood-based microfibrillated cellulose and nanofibrillated cellulose, and applications relating to papermaking: a review. Cellulose 23, 93–123. https://doi.org/10.1007/s10570-015-0798-5.

Pääkko, M., Ankerfors, M., Kosonen, H., et al., 2007. Enzymatic hydrolysis combined with mechanical shearing and high-pressure homogenization for nanoscale cellulose fibrils and strong gels. Enzymatic hydrolysis combined with mechanical shearing and high-pressure homogenization for nanoscale cellulose fibrils and strong gels. Biomacromolecules 8, 1934–1941. https://doi.org/10.1021/bm061215p.

Parit, M., Saha, P., Davis, V.A., Jiang, Z., 2018. Transparent and homogenous cellulose Nanocrystal/Lignin UV-Protection films. ACS Omega 3, 10679–10691. https://doi.org/10.1021/acsomega.8b01345.

Patiño-Masó, J., Serra-Parareda, F., Tarrés, Q., et al., 2019. TEMPO-oxidized cellulose nanofibers: a potential bio-based superabsorbent for diaper production. Nanomaterials. https://doi.org/10.3390/nano9091271.

Pennells, J., Godwin, I.D., Amiralian, N., Martin, D.J., 2020. Trends in the production of cellulose nanofibers from non-wood sources. Cellulose 27, 575–593. https://doi.org/10.1007/s10570-019-02828-9.

Pinto, L.O., Bernardes, J.S., Rezende, C.A., 2019. Low-energy preparation of cellulose nanofibers from sugarcane bagasse by modulating the surface charge density. Carbohydr. Polym. 218, 145–153. https://doi.org/10.1016/j.carbpol.2019.04.070.

Pirich, C.L., Picheth, G.F., Fontes, A.M., et al., 2020. Disruptive enzyme-based strategies to isolate nanocelluloses: a review. Disruptive enzyme-based strategies to isolate nanocelluloses: a review. Cellulose 27, 5457–5475. https://doi.org/10.1007/s10570-020-03185-8.

Puangsin, B., Fujisawa, S., Kuramae, R., et al., 2013. TEMPO-mediated oxidation of Hemp Bast Holocellulose to prepare cellulose nanofibrils dispersed in water. TEMPO-Mediated oxidation of Hemp Bast Holocellulose to prepare cellulose nanofibrils dispersed in water. J. Polym. Environ. 21, 555–563. https://doi.org/10.1007/s10924-012-0548-9.

Qua, E.H., Hornsby, P.R., Sharma, H.S.S., Lyons, G., 2011. Preparation and characterisation of cellulose nanofibres. J. Mater. Sci. 46, 6029–6045. https://doi.org/10.1007/s10853-011-5565-x.

Ramamoorthy, S.K., Skrifvars, M., Persson, A., 2015. A review of natural fibers used in biocomposites: plant, animal and regenerated cellulose fibers. Polym Rev 55, 107–162.

Rodionova, G., Saito, T., Lenes, M., et al., 2013. TEMPO-mediated oxidation of Norway spruce and Eucalyptus pulps: preparation and characterization of nanofibers and nanofiber dispersions. J. Polym. Environ. https://doi.org/10.1007/s10924-012-0483-9.

Rohit, K., Dixit, S., 2016. A review - future aspect of natural Fiber reinforced composite. Polym from Renew Resour 7, 43–60.

Rojo, E., Peresin, M.S., Sampson, W.W., et al., 2015. Comprehensive elucidation of the effect of residual lignin on the physical, barrier, mechanical and surface properties of nanocellulose films. Comprehensive elucidation of the effect of residual lignin on the physical, barrier, mechanical and surface properties of nanocellulose films. Green Chem. 17, 1853–1866. https://doi.org/10.1039/c4gc02398f.

Saito, T., Isogai, A., 2004. TEMPO-mediated oxidation of native cellulose. The effect of oxidation conditions on chemical and crystal structures of the water-insoluble fractions. Biomacromolecules 5, 1983–1989. https://doi.org/10.1021/bm0497769.

Saito, T., Kimura, S., Nishiyama, Y., Isogai, A., 2007. Cellulose nanofibers prepared by TEMPO-mediated oxidation of native cellulose. Biomacromolecules 8, 2485–2491. https://doi.org/10.1021/bm0703970.

Saleem, M.H., Ali, S., Rehman, M., et al., 2020. Jute: a potential candidate for phytoremediation of metals—a review. Jute: a potential candidate for phytoremediation of metals—a review. Plants 9, 1–14. https://doi.org/10.3390/plants9020258.

Salminen, R., Reza, M., Pääkkönen, T., et al., 2017. TEMPO-mediated oxidation of microcrystalline cellulose: limiting factors for cellulose nanocrystal yield. TEMPO-mediated oxidation of microcrystalline cellulose: limiting factors for cellulose nanocrystal yield. Cellulose 24, 1657–1667. https://doi.org/10.1007/s10570-017-1228-7.

Sanchez-Salvador, J.L., Monte, M.C., Batchelor, W., et al., 2020. Characterizing highly fibrillated nanocellulose by modifying the gel point methodology. characterizing

highly fibrillated nanocellulose by modifying the gel point methodology. Carbohydr. Polym. 227, 115340 https://doi.org/10.1016/j.carbpol.2019.115340.
Sbiai, A., Kaddami, H., Sautereau, H., et al., 2011. TEMPO-mediated oxidation of lignocellulosic fibers from date palm leaves. TEMPO-mediated oxidation of lignocellulosic fibers from date palm leaves. Carbohydr. Polym. 86, 1445–1450. https://doi.org/10.1016/j.carbpol.2011.06.005.
Segal, L., Creely, J.J., Martin, A.E., Conrad, C.M., 1959. An empirical method for estimating the degree of crystallinity of native cellulose using the X-Ray diffractometer. Text Res. J. 29, 786–794. https://doi.org/10.1177/004051755902901003.
Serra, A., González, I., Oliver-Ortega, H., et al., 2017. Reducing the amount of catalyst in TEMPO-oxidized cellulose nanofibers: effect on properties and cost. Polymers (Basel). https://doi.org/10.3390/polym9110557.
Serra-Parareda, F., Tarrés, Q., Pèlach, M.À, et al., 2021. Monitoring fibrillation in the mechanical production of lignocellulosic micro/nano fi bers from bleached spruce thermomechanical pulp. monitoring fibrillation in the mechanical production of lignocellulosic micro/nano fi bers from bleached spruce thermomechanical pulp. Int. J. Biol. Macromol. 178, 354–362. https://doi.org/10.1016/j.ijbiomac.2021.02.187.
Sharma, A., Chaudhary, R., 2020. Review of effects of Fiber content and Fiber length on the mechanical properties of biocomposites. Int J Mech Prod Eng Res Dev 10, 12523–12532. https://doi.org/10.24247/ijmperdjun20201192.
Shinoda, R., Saito, T., Okita, Y., Isogai, A., 2012. Relationship between length and degree of polymerization of TEMPO-Oxidized cellulose nanofibrils. Biomacromolecules 13, 842–849.
Siqueira, G., Tapin-Lingua, S., Bras, J., et al., 2010. Morphological investigation of nanoparticles obtained from combined mechanical shearing, and enzymatic and acid hydrolysis of sisal fibers. Morphological investigation of nanoparticles obtained from combined mechanical shearing, and enzymatic and acid hydrolysis of sisal fibers. Cellulose 17, 1147–1158. https://doi.org/10.1007/s10570-010-9449-z.
Sjöstedt, A., Wohlert, J., Larsson, P.T., Wågberg, L., 2015. Structural changes during swelling of highly charged cellulose fibres. Cellulose 22, 2943–2953. https://doi.org/10.1007/s10570-015-0701-4.
Sjöström, E., Westermark, U., 1999. Chemical composition of wood and pulps: basic constituents and their distribution. In: Analytical Methods in Wood Chemistry, Pulping, and Papermaking. Springer, pp. 1–19.
Song, X., Jiang, Y., Rong, X., et al., 2016. Surface characterization and chemical analysis of bamboo substrates pretreated by alkali hydrogen peroxide. Surface characterization and chemical analysis of bamboo substrates pretreated by alkali hydrogen peroxide. Bioresour. Technol. 216, 1098–1101. https://doi.org/10.1016/j.biortech.2016.06.026.
Souza, S.F., Mariano, M., De Farias, M.A., Bernardes, J.S., 2019. Effect of depletion forces on the morphological structure of carboxymethyl cellulose and micro/nano cellulose fiber suspensions. J. Colloid Interface Sci. 538, 228–236. https://doi.org/10.1016/j.jcis.2018.11.096.
Spence, K.L., Venditti, R.A., Rojas, O.J., et al., 2011. A comparative study of energy consumption and physical properties of microfibrillated cellulose produced by different processing methods. A comparative study of energy consumption and physical properties of microfibrillated cellulose produced by different processing methods. Cellulose 18, 1097–1111. https://doi.org/10.1007/s10570-011-9533-z.
Sridach, W., 2010. The environmentally benign pulping process of non-wood fibers. Suranaree J Sci Technol 17, 105–123.
Sun, B., Gu, C., Ma, J., Liang, B., 2005. Kinetic study on TEMPO-mediated selective oxidation of regenerated cellulose. Cellulose 12, 59–66. https://doi.org/10.1007/s10570-004-0343-4.
Sundholm, J., 1999. Mechanical pulping. Fapet Oy.
Tarrés, Q., Ehman, N.V., Vallejos, M.E., et al., 2016a. The feasibility of incorporating cellulose micro/nanofibers in papermaking processes: the relevance of enzymatic hydrolysis. the feasibility of incorporating cellulose micro/nanofibers in papermaking processes: the relevance of enzymatic hydrolysis. Cellulose 23, 795–807. https://doi.org/10.1590/S1516-89132007000100003.
Tarrés, Q., Saguer, E., Pèlach, M.A., et al., 2016b. The feasibility of incorporating cellulose micro/nanofibers in papermaking processes: the relevance of enzymatic hydrolysis. the feasibility of incorporating cellulose micro/nanofibers in papermaking processes: the relevance of enzymatic hydrolysis. Cellulose 23, 1433–1445. https://doi.org/10.1007/s10570-016-0889-y.
Tarrés, Q., Boufi, S., Mutjé, P., Delgado-Aguilar, M., 2017a. Enzymatically hydrolyzed and TEMPO-oxidized cellulose nanofibers for the production of nanopapers: morphological, optical, thermal and mechanical properties. Cellulose. https://doi.org/10.1007/s10570-017-1394-7.
Tarrés, Q., Ehman, N.V., Vallejos, M.E., et al., 2017b. Lignocellulosic nanofibers from triticale straw: The influence of hemicelluloses and lignin in their production and properties. Lignocellulosic nanofibers from triticale straw: The influence of hemicelluloses and lignin in their production and properties. Carbohydr. Polym. 163, 20–27. https://doi.org/10.1016/j.carbpol.2017.01.017.
Tarrés, Q., Espinosa, E., Domínguez-Robles, J., et al., 2017c. The suitability of banana leaf residue as raw material for the production of high lignin content micro/nano fibers: from residue to value-added products. the suitability of banana leaf residue as raw material for the production of high lignin content micro/nano fibers: from residue to value-added products. Ind. Crops Prod. 99, 27–33. https://doi.org/10.1016/j.indcrop.2017.01.021.
Tarrés, Q., Mutjé, P., Delgado-Aguilar, M., 2019. Towards the development of highly transparent, flexible and water-resistant bio-based nanopapers: tailoring physico-mechanical properties. Cellulose 26, 6917–6932. https://doi.org/10.1007/s10570-019-02524-8.
Torres, C.E., Negro, C., Fuente, E., Blanco, A., 2012. Enzymatic approaches in paper industry for pulp refining and biofilm control. Appl. Microbiol. Biotechnol. 96, 327–344. https://doi.org/10.1007/s00253-012-4345-0.
Trakulvichean, S., Chaiprasert, P., Otmakhova, J., 2019. Integrated economic and environmental assessment of biogas and bioethanol production from cassava cellulosic waste. Waste Biomass Valorization 10, 691–700. https://doi.org/10.1007/s12649-017-0076-x.
Varanasi, S., He, R., Batchelor, W., 2013. Estimation of cellulose nanofibre aspect ratio from measurements of fibre suspension gel point. Cellulose 20, 1885–1896. https://doi.org/10.1007/s10570-013-9972-9.
Wen, Y., Yuan, Z., Liu, X., et al., 2019. Preparation and characterization of lignin-containing cellulose nanofibril from poplar high-yield pulp via TEMPO-Mediated oxidation and homogenization. preparation and characterization of lignin-containing cellulose nanofibril from poplar high-yield pulp via TEMPO-Mediated oxidation and homogenization. ACS Sustain. Chem. Eng. 7, 6131–6139. https://doi.org/10.1021/acssuschemeng.8b06355.
Winter, H.T., Cerclier, C., Delorme, N., et al., 2010. Improved colloidal stability of bacterial cellulose nanocrystal suspensions for the elaboration of spin-coated cellulose-based model surfaces. improved colloidal stability of bacterial cellulose nanocrystal suspensions for the elaboration of spin-coated cellulose-based model surfaces. Biomacromolecules 11, 3144–3151. https://doi.org/10.1021/bm100953f.
Zhang, H., Zhao, C., Li, Z., Li, J., 2016. The fiber charge measurement depending on the poly-DADMAC accessibility to cellulose fibers. Cellulose 23, 163–173.
Zhao, X., Zhang, L., Liu, D., 2012. Biomass recalcitrance. Part I: the chemical compositions and physical structures affecting the enzymatic hydrolysis of lignocellulose. Biofuels, Bioprod Biorefining 6, 465–482. https://doi.org/10.1002/bbb.
Zhou, Y., Saito, T., Bergström, L., Isogai, A., 2018. Acid-free preparation of cellulose nanocrystals by TEMPO oxidation and subsequent cavitation. Biomacromolecules 19, 633–639. https://doi.org/10.1021/acs.biomac.7b01730.